nature neuroscience

The nuclear import of Frizzled2-C by Importins-β11 and α2 promotes postsynaptic development

Timothy J Mosca[1–3] & Thomas L Schwarz[1,2]

Synapse-to-nucleus signaling is critical for synaptic development and plasticity. In *Drosophila*, the ligand Wingless causes the C terminus of its Frizzled2 receptor (Fz2-C) to be cleaved and translocated from the postsynaptic density to nuclei. The mechanism of nuclear import is unknown and the developmental consequences of this translocation are uncertain. We found that Fz2-C localization to muscle nuclei required the nuclear import factors Importin-β11 and Importin-α2 and that this pathway promoted the postsynaptic development of the subsynaptic reticulum (SSR), an elaboration of the postsynaptic plasma membrane. *importin-β11* (*imp-β11*) and *dfz2* mutants had less SSR, and some boutons lacked the postsynaptic marker Discs Large. These developmental defects in *imp-β11* mutants could be overcome by expression of Fz2-C fused to a nuclear localization sequence that can bypass Importin-β11. Thus, Wnt-activated growth of the postsynaptic membrane is mediated by the synapse-to-nucleus translocation and active nuclear import of Fz2-C via a selective Importin-β11/α2 pathway.

Communication between the synapse and nucleus is essential for proper synaptic regulation, and several pathways have been identified in which synaptic signals are translated into nuclear instructions. Importins facilitate protein entry into the nucleus and can be critical for conveying these synapse-to-nucleus signals[1,2]. In classical nuclear import, cargo binds to an Importin-α and subsequent binding of an Importin-β allows the complex to pass through the nuclear pore[3]. In neurons, importins mediate signals from sites of axonal injury[4], signals generated during LTP and other forms of synaptic plasticity, and signals required for photoreceptor axon targeting[5,6]. Importins are emerging as a critical nexus of regulation between synaptic signals and the nucleus.

Wnt pathways are implicated in synaptic development and can include nuclear responses[7]. The best-studied nuclear response entails β-catenin, which does not require an importin for nuclear entry[8]. In other pathways, the *Drosophila* Wnt receptor Fz2 and the unrelated mammalian Wnt receptor Ryk are cleaved and their liberated C termini (Fz2-C or Ryk-C) translocate directly to the nucleus[9,10]. The mechanism of nuclear import of these receptor-derived peptides is not known, but Fz2-C is of particular interest as it potentially links activity-dependent release of Wingless (the *Drosophila* Wnt ligand) from the presynaptic motor neuron to synaptic plasticity[10–12].

Deciphering the functional importance of nuclear Fz2-C translocation has been complicated by the myriad of other potential Wnt signaling pathways that may also be present. Although multiple phenotypes have been reported for *wg* and *dfz2* at the fly neuromuscular junction (NMJ), including changes in synapse size and number, neuronal microtubule organization, and postsynaptic development[11,13,14], it has not been possible to determine which, if any, can be attributed to nuclear translocation of Fz2-C. Recently, we found that defects in bouton number and size and microtubules were accounted for by a local presynaptic pathway that is largely independent of Wingless/Fz2 signaling in the muscle[13]. Wingless signaling, however, is also implicated in some postsynaptic phenotypes that might be a result of signaling in muscles. In addition to glutamate receptor localization, postsynaptic development includes formation of the subsynaptic reticulum (SSR), a complex array of folds in the plasma membrane that are potentially analogous to dendritic spines or the junctional folds of the vertebrate NMJ[15]. Mutations in *wg* reduce this SSR[14]. Thus, understanding the precise contributions of pre- and postsynaptic Wnt signaling is critical for a thorough understanding of synapse development. We found that Importin-β11 and Importin-α2 can mediate synapse-to-nucleus signaling. Mutations in these importins selectively blocked the nuclear translocation of Fz2-C and revealed its requirement for Wingless-stimulated growth of the SSR and postsynaptic specializations.

RESULTS

Importins-β11 and α2 are required for Fz2-C nuclear import

Nuclear import can proceed via an Importin-α and Importin-β acting jointly or by an Importin-β alone[3]. Our previous work determined that Importin-β11 was expressed in muscle nuclei (**Fig. 1**)[16], but we did not examine Importin-α expression in these muscles. Of the three *Drosophila* Importin-α homologs[17], neither Importin-α1 nor Importin-α3 could be detected immunocytochemically in muscle nuclei (**Fig. 1c**,**d**,**i**,**j**). Importin-α2 immunoreactivity, however, was present in wild-type, but not *importin-α2* (*imp-α2*, also known as *Pen*) mutant, nuclei (**Fig. 1e**–**h**). Nonspecific immunoreactivity was seen at the NMJ

[1]The F.M. Kirby Neurobiology Center, Children's Hospital Boston, Boston, Massachusetts, USA. [2]Department of Neurobiology, Harvard Medical School, Boston, Massachusetts, USA. [3]Present address: Stanford University, Department of Biology, Stanford, California, USA. Correspondence should be addressed to T.L.S. (thomas.schwarz@childrens.harvard.edu).

Received 19 January; accepted 4 June; published online 4 July 2010; doi:10.1038/nn.2593

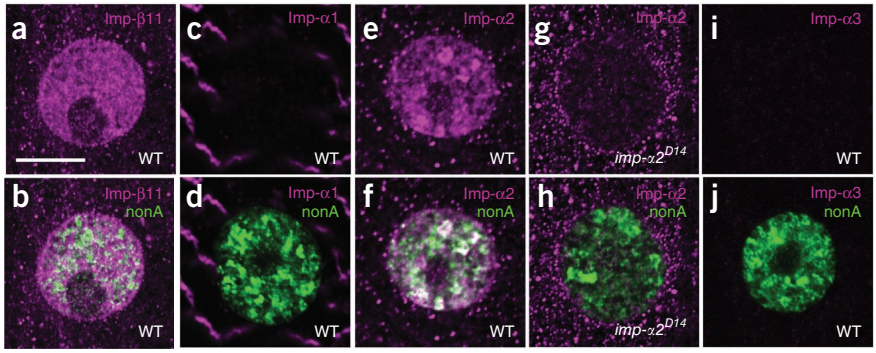

Figure 1 Importin-β11 and Importin-α2 are expressed in *Drosophila* muscle nuclei. (**a**–**j**) Representative confocal images of wild-type (*y,w*; *FRT42D*; *+*; *+*) nuclei (**a**–**f**,**i**,**j**) or *imp-α2* null mutant (*y,w*; *imp-α2*^{D14}; *+*; *+*) nuclei (**g**,**h**) stained with antibodies to an importin (magenta) and to the nuclear marker nonA (green). Importin-β11 staining was observed at the nuclear envelope and in the nucleus (**a**,**b**). Antibodies to Importin-α1 nonspecifically labeled Z-bands but staining was undetectable in the nucleus (**c**,**d**). Importin-α2 staining was observed in the nucleus (**e**,**f**). In *imp-α2* null mutant nuclei, antibodies to Importin-α2 did not label muscle nuclei, indicating that the nuclear staining in **e** and **f** was specific for Importin-α2 (**g**,**h**). Nonspecific puncta in the cytoplasm persisted, however, in the mutant. (**i**,**j**) Antibodies to Importin-α3 did not stain wild-type muscles, although the antibody did recognize Importin-α3 in neuronal tissues that are known to express Importin-α3 (data not shown). Scale bar represents 10 μm.

of both wild-type and *imp-α2* mutant larvae (data not shown), which prevented us from determining whether Importin-α2 was also at the synapse.

Muscle expression of Importin-α2 and Importin-β11 led us to hypothesize that they may mediate the nuclear entry of Fz2-C. To begin this analysis, we first reexamined the question of Fz2 expression, cleavage and translocation in the muscle. We used antibodies raised to the C terminus of the receptor[10] to examine the subcellular localization of Fz2-C in larval muscle. As has been shown previously[10], the antibody recognized neuromuscular junctions and puncta in muscle nuclei (**Supplementary Fig. 1**). The specificity of the staining was confirmed by its absence in *dfz2* null mutants (**Supplementary Fig. 1**)[10,18]. To address the nuclear import of the C terminus independently of the Fz2-C antibody, we overexpressed a transgenic Fz2 receptor with a C-terminal FLAG epitope in muscle. Antibodies to FLAG labeled synapses as well as puncta at the nuclear envelope and in the nucleus itself (**Supplementary Fig. 1**). Furthermore, when immunoblots of body-wall lysates from these larvae were probed with a FLAG antibody, two species were detected: a full-length, ~85-kDa band and a ~15-kDa band, likely corresponding to the cleaved C-terminal peptide. These findings confirmed previous observations that the C terminus of the Fz2 receptor is cleaved and imported into the nucleus[10].

To determine whether Importin-β11 or Importin-α2 are required for nuclear Fz2-C translocation, we examined mutants of each for defects in Fz2-C localization (**Fig. 2**). Muscle nuclei of either *imp-β11* or *imp-α2* mutant larvae held 85% fewer puncta that were immunoreactive for Fz2-C than wild type (**Fig. 2a**–**h**,**k**). In 40% of mutant nuclei, the absence of nuclear Fz2-C puncta was accompanied by the presence of puncta at or outside the nuclear envelope (**Fig. 2f**,**h**). This perinuclear accumulation, never seen in wild type, is consistent with a deficiency in active nuclear import of Fz2-C. Moreover, in wild-type genetic backgrounds, the number of nuclear Fz2-C puncta could be nearly tripled by neuronal overexpression of the ligand Wingless (**Fig. 2k**), consistent with previous observations[10]. In *imp-β11* larvae, however, neuronal Wingless overexpression could not restore Fz2-C to muscle nuclei ($P > 0.2$; **Fig. 2k** and **Supplementary Fig. 2**). In contrast with *imp-β11* or *imp-α2* mutants, *Kap-α1* (*importin-α1*) mutants had normal levels of nuclear Fz2-C (wild type = 0.93 ± 0.03 puncta, $n = 3$ animals, 143 nuclei; *Df(3L)α1S1* = 1.2 ± 0.10 puncta, $n = 4$ animals, 249 nuclei; $P > 0.3$).

Nuclear Fz2-C in *imp-β11* or *imp-α2* mutants could be restored to 71% and 85%, respectively, of wild-type levels by expression of the corresponding importin in muscle (**Fig. 2k** and **Supplementary Fig. 2**). Muscle overexpression of Ketel, the *Drosophila* homolog of Importin-β1, could not rescue the *imp-β11* mutant phenotype, suggesting specificity for Importin-β11 ($P > 0.2$; **Fig. 2k**). Similarly, expression of the importins in the nervous system did not restore Fz2-C to muscle nuclei ($P > 0.2$; **Fig. 2k**). Thus, Fz2-C requires Importin-β11 and Importin-α2 in muscle for nuclear localization, which is consistent with them having a direct role in nuclear import of Fz2-C.

The *imp-β11* mutant could be selectively defective in Fz2-C import or generally impaired in nuclear import. We therefore examined three other proteins that translocate from the synapse to the nucleus. Nanos, an RNA binding protein[19], was still present in *imp-β11* mutant muscle nuclei (**Fig. 2i,j**). Similarly, pMad, the downstream effector of bone morphogenic protein (BMP) signaling at the NMJ, was properly imported into *imp-β11* mutant nuclei[16]. In addition, the NF-κB transcription factor Dorsal[20] properly localized to the NMJ (data not shown) and muscle nuclei (**Supplementary Fig. 3**). This staining was specific for Dorsal, as it was undetectable in *dorsal* null mutants (**Supplementary Fig. 3**). Other nuclear proteins were also imported in *imp-β11* mutants, including nonA, a pan-nuclear RNA-binding protein, muscle-expressed green fluorescent protein (GFP)-tagged with a nuclear localization sequence, Importin-α2, and Importin-β1 (**Supplementary Fig. 3**). Thus, general nuclear import is not impaired in the *imp-β11* mutant and, although other unidentified proteins may require Importin-β11 for import, the absence of Fz2-C from muscle nuclei is a selective phenotype, even among synapse-to-nucleus signaling molecules.

Wnt pathway components persist in Importin mutants

The absence of nuclear Fz2-C localization need not be, a priori, a direct defect in nuclear import; mislocalization or loss of expression of Wnt signaling components in *imp-β11* or *imp-α2* could reduce nuclear Fz2-C as a secondary consequence. We therefore examined Wingless, Fz2 and dGRIP, a scaffold protein[11,14] at the fly NMJ, and found no detectable change in their localization or levels of expression in either *imp-β11* or *imp-α2* (**Fig. 3a**–**r**). Thus, the lack of nuclear Fz2-C in the *imp-β11* or *imp-α2* mutants cannot be accounted for by the loss of upstream components of the pathway.

To determine whether receptor endocytosis was blocked, we examined the localization of Fz2 with antibodies to its N terminus (Fz2-N). Antibodies to Fz2-N label both the NMJ and a ring that appears to be at or tightly associated with the nuclear envelope and is dependent on endocytosis and receptor trafficking[10]. In all genotypes, this ring of Fz2-N staining outlined muscle nuclei (**Fig. 3s**–**x**); thus, endocytosis and relocation to the nuclear envelope of the Fz2-N portion occurred in the absence of Importin-β11 or Importin-α2. Moreover, cleavage of Fz2-C from Fz2-N also occurred in the mutants; the Fz2-N-associated nuclear envelope was not stained by antibodies to Fz2-C (compare **Figs. 2** and **3**). Fz2-C, although transported to the vicinity of the nucleus in the

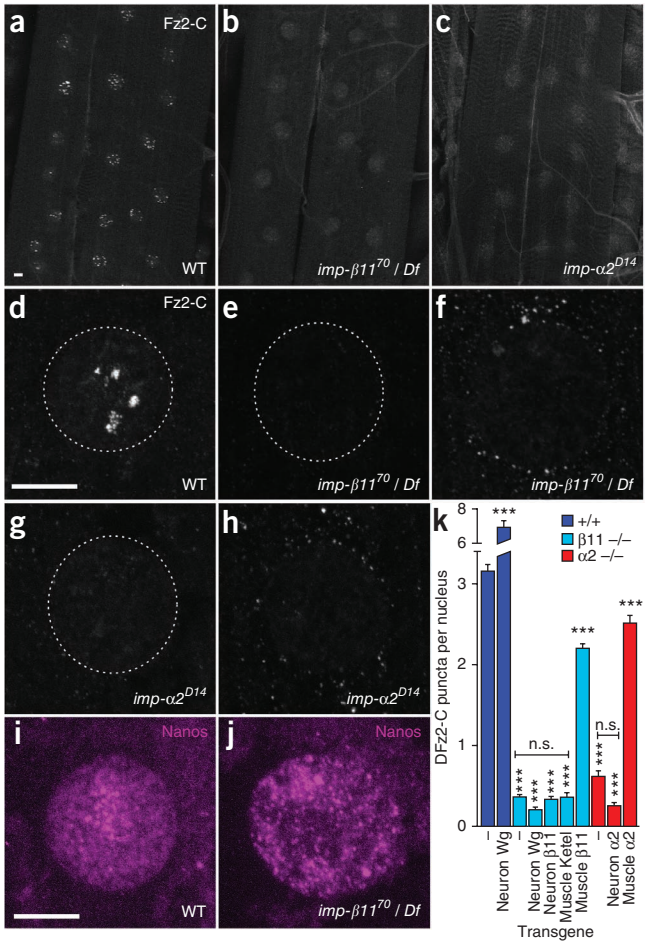

Figure 2 Importin-β11 and Importin-α2 are required for proper nuclear import of Fz2-C. (**a**–**c**) Representative wide-field image stacks of muscles 6 and 7 in wild-type (*y,w*; *FRT42D; +; +*; **a**), *imp-β11* mutant (*y,w*; *imp-β11*^{70} / *Df; +; +*; **b**) and *imp-α2* mutant (*y,w*; *imp-α2*^{D14}*; +; +*; **c**) third instar larvae stained with antibodies to the C terminus of Fz2. Immunoreactive puncta are evident in nuclei (dashed circle) in wild type, but not *imp-β11* or *imp-α2* mutants. (**d**–**h**) Representative individual nuclei stained with an antibody to Fz2-C. The nuclear puncta of Fz2-C present in wild type (**d**) were absent from *imp-β11* (**e**,**f**) or *imp-α2* (**g**,**h**) mutant nuclei. Though lacking internal Fz2-C puncta, some mutant nuclei had punctate immunoreactivity at the nuclear envelope, similar to those shown in **f** and **h**. (**i**,**j**) Nuclei immunostained for Nanos (magenta), an RNA binding protein present at the NMJ and in nuclei of both wild-type (**i**) and *imp-β11* mutants (**j**), illustrating the specificity of the Fz2-C phenotype. Scale bars represent 10 μm. (**k**) Quantification of Fz2-C nuclear puncta in third instar larval muscles showing the mutant phenotypes, as well as their rescue by the transgenic expression of the specific importin in the muscle. Colors indicate the genetic background in which the marked transgenes were expressed. Genotypes are as follows: +/+ (*y,w*; *FRT42D*; *+*; *+*); Neuron Wingless (*y,w*; *+*; *elav-GAL4 / UAS-Wingless*; *+*); β11 –/– (*y,w*; *imp-β11*^{70} / *Df*; *+*; *+*); β11 –/– Neuron Wingless (*y,w*; *imp-β11*^{70} / *Df*; *elav-GAL4 / UAS-Wingless*; *+*); β11 –/– Neuron β11 (*y,w*; *imp-β11*^{70} / *Df*; *elav-GAL4 / UAS–imp-β11–eGFP*; *+*); β11 –/– Muscle β11 (*y,w*; *imp-β11*^{70} / *Df*; *24B-GAL4 / UAS– imp-β11–eGFP*; *+*); β11 –/– Muscle Ketel (*y,w*; *imp-β11*^{70} / *Df*; *24B-GAL4 / UAS-Ketel*; *+*); α2 –/– (*y,w*; *imp-α2*^{D14}; *+*; *+*); α2 –/– Neuron α2 (*y,w*; *imp-α2*^{D14}; *elav-GAL4 / UAS-imp-α2*; *+*); α2 –/– Muscle α2 (*y,w*; *imp-α2*^{D14}; *24B-GAL4 / UAS-imp-α2*; *+*). Substantial rescue was observed with restored muscle, but not neuronal, expression of either importin in the respective mutant background. ***$P < 0.0001$ compared with wild type. Error bars represent s.e.m.

absence of Importin-β11 or Importin-α2, was separately localized in puncta outside the nuclear envelope (**Fig. 2**). As previously reported[10], endogenous Fz2 levels were too low to be detected on immunoblots by available antibodies for further confirmation of receptor cleavage. Thus, importins appear to be specifically required for Fz2-C translocation across the nuclear envelope but, despite associating with receptors at the synapse, are not required for Fz2-C generation or movement through the cytoplasm.

An Importin/Fz2-C complex at synapses and in the cytosol

The requirement for Importin-β11 and Importin-α2 in Fz2-C nuclear import raises the possibility of their physical interaction at the synapse, in the cytosol or at the nuclear pore. As the Importin-β11, Importin-α2 and Fz2-C antisera were all from rabbits, immunocytochemical colocalization of endogenous proteins was not practical. We therefore coexpressed GFP-tagged Importin-β11 and Fz2 with a C-terminal FLAG tag in larval muscles. Both tagged proteins retain their functions[16,21] and Fz2-FLAG distribution in muscle resembled that of endogenous Fz2 (**Supplementary Fig. 1**).

Expressed alone, Importin-β11–enhanced GFP (eGFP) was diffusely cytoplasmic with occasional cytosolic puncta and prominent nuclear labeling (**Fig. 4a–c**). It was not detected at the NMJ (**Fig. 4a–c**). In contrast, when coexpressed with Fz2-FLAG, the two extensively colocalized in the postsynaptic region (**Fig. 4d–f**); thus, overexpression of Fz2-FLAG recruited Importin-β11 to the synapse.

Fz2-FLAG and Importin-β11–eGFP also colocalized in cytoplasmic puncta (**Fig. 4d–f**) that are likely to represent internalized C-terminal peptides en route to the nucleus[10,11]. These FLAG- and eGFP-positive puncta were frequently near the nucleus (**Fig. 4g–i**). The colocalization of Importin-β11 and the FLAG tag at synapses, in the cytoplasm and around the nucleus suggests that Fz2-C traffics in association with Importin-β11 to ensure nuclear entry.

We also examined whether the importins and receptor would co-immunoprecipitate. Antibodies to FLAG immunoprecipitated Importin-β11–GFP from third instar body-wall preparations that coexpressed Fz2-FLAG and Importin-β11–eGFP, but not when Importin-β11–eGFP was expressed alone (**Fig. 4j**). Although co-immunoprecipitation of endogenous Importin-β11 and Importin-α2 could not be detected from either S2 cells or wild-type body walls (data not shown), endogenous Importin-α2 did coprecipitate with Fz2-FLAG, but only when Importin-β11–eGFP was also expressed (**Fig. 4j**). Thus, Fz2 can form a complex containing both importins, and Importin-β11 may be necessary to stabilize the incorporation of Importin-α2 into the complex.

NLS-tagged Fz2-C is imported independently of Importin-β11

Although Importin-β11 was required for normal Fz2-C import, we attempted to bypass that requirement. In larval muscles, we expressed the C-terminal 88 amino acids of Fz2-C with a nuclear localization signal (NLS) and a myc epitope (**Fig. 5a**) on its N terminus so as not to interfere with the PDZ-binding domain[10]. Attaching an NLS to cargoes can allow for import by alternative routes such as Importin-β1 (ref. 22).

In addition to diffuse cytoplasmic myc immunoreactivity, as seen previously[10], we observed enrichment of myc-NLS–Fz2-C around synaptic boutons (**Fig. 5b,c**), probably as a result of binding via the PDZ-binding domain. We also observed nuclear myc-immunoreactivity in both wild-type and *imp-β11* mutants (**Fig. 5d–f**). The nuclear immunoreactivity was punctate, but these puncta were smaller than endogenous Fz2-C puncta and most abundant near the nucleolus. Thus, the NLS-fused Fz2-C (similar to NLS-GFP; **Supplementary Fig. 3**) enters the nucleus even in the absence of

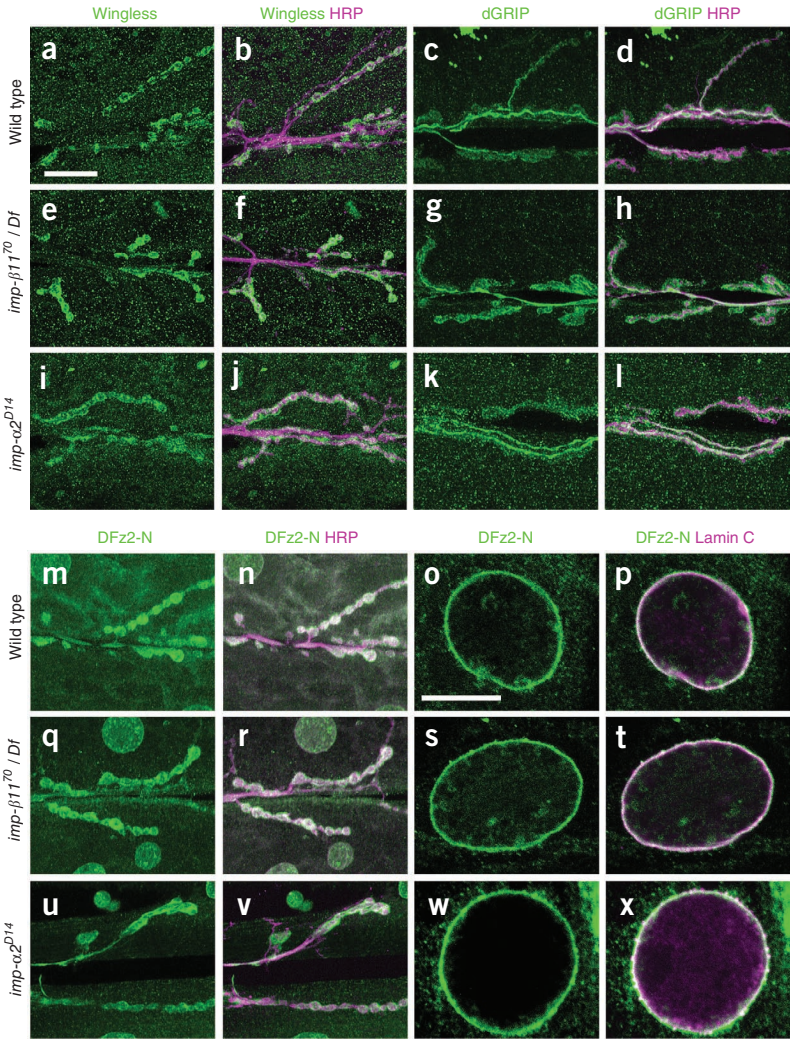

Figure 3 Wnt pathway components are properly localized in importin mutants. (**a**–**r**) Representative confocal images of the NMJ at muscles 6 and 7 in the indicated genotypes, immunostained as indicated with antibodies to HRP (magenta) to mark the neuronal endings. Neither importin mutant prevented Wingless ligand localization to synaptic boutons, dGRIP localization to synapses or Frizzled2 receptor localization to the synapse. Antibodies to the N terminus (Fz2-N) and C terminus (Fz2-C; data not shown) gave equivalent results. (**s**–**x**) Single confocal slices through the equator of individual third-instar muscle nuclei in the indicated genotypes and stained with the antibody to Fz2-N (green) and an antibody to Lamin C (magenta) to mark the nuclear envelope. Perinuclear staining in each genotype indicates endocytosis and trafficking of the Fz2 receptor to the nuclear envelope. Scale bar represents 10 μm. Genotypes: wild type (*y,w*; *FRT42D*; *+*; *+*), *imp-β11*^{70} / *Df* (*y,w*; *imp-β11*^{70} / *Df*; *+*; *+*), *imp-α2*^{D14} (*y,w*; *imp-α2*^{D14}; *+*; *+*).

Importin-β11; this raised the possibility that myc-NLS–Fz2-C could functionally substitute for normal Fz2 signaling.

Nuclear Fz2-C does not regulate presynaptic structure

The ability to selectively prevent the nuclear entry of Fz2-C permitted the investigation of its developmental consequences, as distinguished from those of other Fz2-activated pathways. It was previously hypothesized that Fz2-C import controls presynaptic bouton size, number and cytoskeletal organization through a retrograde, muscle-derived signal[10]. However, recent work has shown that Wingless-related modulation of these parameters is predominantly explained by presynaptic Fz2 signaling[13]. We examined *imp-β11* and *imp-α2* mutants with regard to these phenotypes to ascertain whether the nuclear Fz2-C pathway was involved.

Defective Wingless signaling alters microtubules in synaptic boutons, as determined by immunostaining for Futsch, the *Drosophila* MAP1B homolog[23,24]. Defects manifest as increased disorganized, unbundled Futsch and fewer Futsch-positive microtubule loops in boutons[13,14]. To determine whether loss of nuclear Fz2-C causes these defects, we examined Futsch in *imp-β11* and *imp-α2* mutants and found that they did not recapitulate the *wg* phenotype. No differences were found in counts of boutons with unbundled Futsch or Futsch-immunoreactive loops (**Supplementary Fig. 4**). We conclude that impaired muscle Fz2-C import does not affect presynaptic microtubule organization.

Mutations in the Wnt pathway decrease the number of synaptic boutons, but increase the number of large (>5 μm diameter) boutons[10,13,14]. *imp-β11* mutants have 30% fewer boutons, but this is a result of a presynaptic function of Importin-β11 (ref. 16). Restoration of presynaptic Importin-β11 expression in *importin-β11* mutants restored bouton numbers despite the nearly complete absence of nuclear Fz2-C in the muscle. Furthermore, *imp-α2* mutants lacked nuclear Fz2-C (**Fig. 2c**,**g**,**h**,**k**), but had normal numbers of boutons (data not shown). Neither of the importin mutants had increased boutons of >5 μm diameter (data not shown). Thus, postsynaptic nuclear Fz2-C signaling appears not to govern the presynaptic phenomena of bouton number, bouton size or microtubule organization.

wg and *dfz2* mutants have errors in postsynaptic specializations

Although we found no role for Fz2-C import in presynaptic development, it is possible that it is involved postsynaptically. In *Drosophila*, the postsynaptic NMJ is organized by Discs Large (DLG), the homolog of mammalian PSD-95 (ref. 25). Normally, postsynaptic DLG surrounds synaptic boutons and active zones align with glutamate receptor clusters[26]. Occasionally, however, so-called 'ghost' boutons are seen where neither DLG nor glutamate receptors are concentrated opposite a bouton. These boutons contain synaptic vesicles, but largely lack active zones[11]. The *wg* pathway has been indirectly implicated in regulating ghost bouton frequency because muscle dGRIP RNA interference increases their numbers and activity-dependent increases in ghost boutons are altered in *wg* mutants[11,12].

To test directly for an effect of the *wg* pathway and specifically Fz2-C nuclear import, we immunostained *wg* and *dfz2* larvae with antibodies to horseradish peroxidase (HRP) and DLG (**Supplementary Fig. 5**) and counted the number of boutons at muscles 6 and 7 lacking surrounding DLG. In wild type, ghost boutons were occasionally seen (**Fig. 6j**) and found to lack apposite glutamate receptors (by GluRIIC staining) and the active zone protein Bruchpilot, but

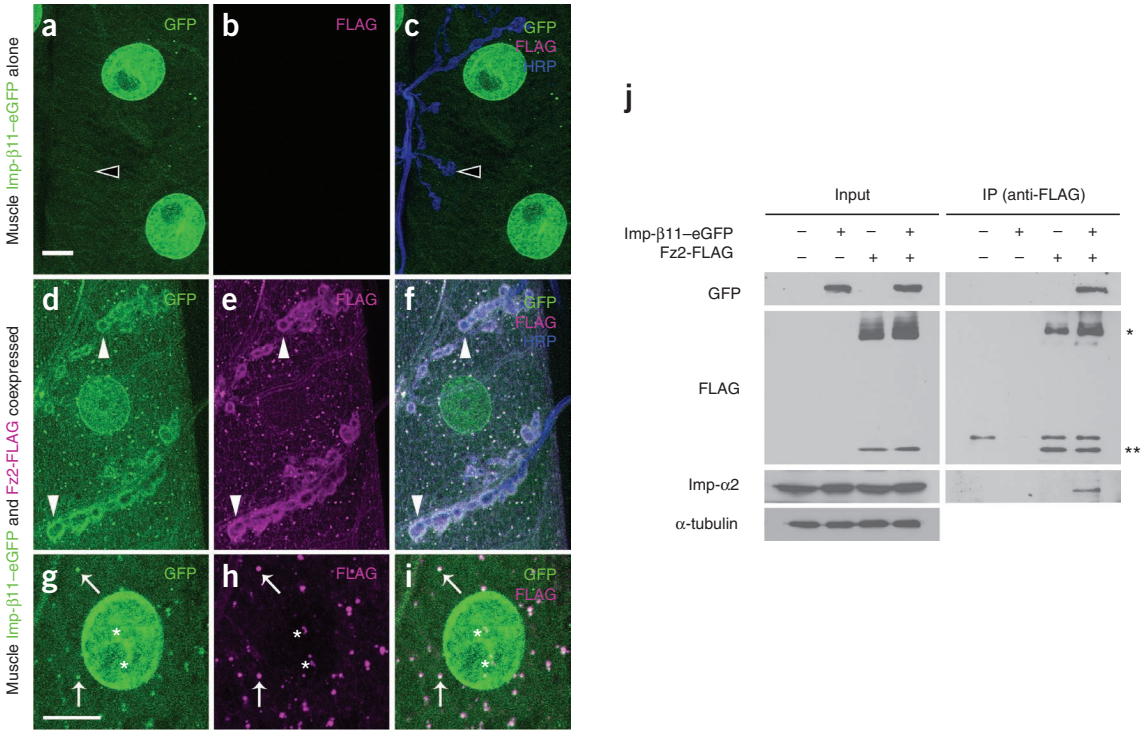

Figure 4 Fz2 colocalizes with and binds Importin-β11 and Importin-α2. (**a**–**c**) Muscles expressing Importin-β11–eGFP (green) alone in *y,w*; *+*; *24B-GAL4 / UAS-Importin-β11-eGFP*; *+* larvae. Importin-β11–eGFP localized to muscle nuclei and diffusely in the cytoplasm, but was not concentrated at the NMJ (stained with antibodies to HRP, blue, open arrowhead). (**d**–**f**) In muscles expressing both Importin-β11–eGFP (green) and Fz2-FLAG (magenta) in *y,w*; *UAS-Fz2-FLAG / +*; *24B-GAL4 / UAS-importin-β11-eGFP*; *+* larvae. Importin-β11 and Fz2 colocalized at the NMJ (filled arrowheads). (**g**–**i**) A single muscle nucleus from a larva coexpressing Importin-β11–eGFP and Fz2-FLAG as in **d**–**f**. Each FLAG-positive Fz2 punctum colocalized with a GFP-positive Importin-β11 punctum (arrows), including puncta in the cytoplasm, at the nuclear envelope and in the nucleus (asterisk). Scale bar represents 10 μm. (**j**) Immunoblots of larvae coexpressing Importin-β11–eGFP and DFz2-FLAG. The proteins were immunoprecipitated with antibodies to FLAG and detected with antibodies to GFP, FLAG or Importin-α2. Expressed Importin-β11–eGFP and endogenous Importin-α2 proteins were co-immunoprecipitated with the receptor. Both the full-length Fz2 (*) and the C terminus (**) were detected by antibodies to FLAG. Antibodies to FLAG also detected a nonspecific background species (middle band). α-tubulin was used as a loading control. All blots except for the Importin-α2 blot were cropped; the full-length blots are presented in **Supplementary Figure 13**.

were Synaptotagmin I immunoreactive. When Wingless and Fz2 signaling were perturbed, ghost bouton frequency increased; in hypomorphic wg^1 mutants, their frequency doubled, whereas their frequency was increased fourfold in the more severe wg^{TS} mutant when the mutant was shifted to a nonpermissive temperature (**Supplementary Fig. 5**). Similarly, the number of ghost boutons increased nearly threefold in *dfz2* mutants (**Supplementary Fig. 5**). Neuronal overexpression of Wingless (**Fig. 2**)[10] and hyperactivity mutations such as eag^1Sh^{KS133} double mutants[12] increased Wingless signaling and nuclear Fz2-C. In these genotypes, ghost boutons were significantly fewer than in wild type ($P < 0.05$; **Supplementary Fig. 5**). Thus, manipulations that decreased Wingless and Fz2 signaling increased the frequency of ghost boutons and those that enhanced signaling diminished their occurrence.

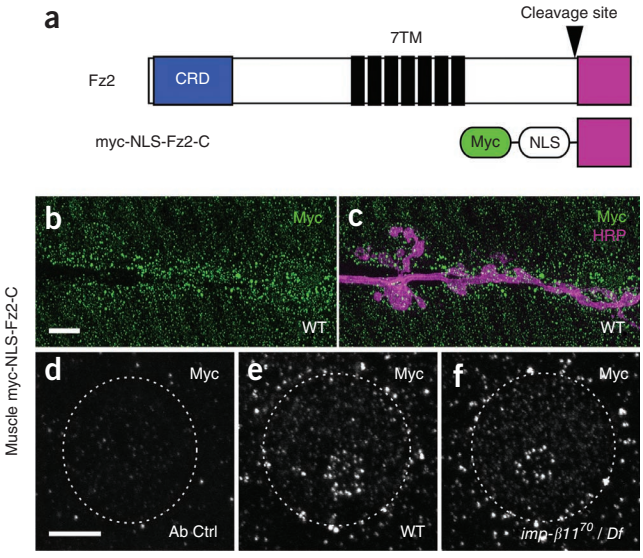

Figure 5 An NLS-tagged, truncated Fz2-C construct localizes to synapses and is imported independently of Importin-β11. (**a**) Organization of the full-length Fz2 protein and the truncated C-terminal construct. For this construct, the sequence after the cleavage site (arrowhead) was cloned behind a classical, monopartite NLS and a myc epitope[10]. CRD, cysteine rich domain; TM, transmembrane domain. (**b**,**c**) Representative confocal images of *w*, *UAS-myc-NLS-Fz2-C*; *+*; *24B-GAL4 / +*; *+* third-instar larval NMJs expressing myc-NLS–Fz2-C in the muscle and stained with an antibodies to myc (green) and HRP (magenta). Myc immunoreactivity appeared to be concentrated near boutons. Scale bar represents 5 μm. (**d**–**f**) Representative single confocal slices through the equator of muscle nuclei (dashed circles) stained with antibodies to myc. In the absence of the transgene (*y,w*; *FRT42D*; *+*; *+*), immunoreactivity was absent (**d**). When myc-NLS–Fz2-C was expressed in wild-type (*w*, *UAS-myc-NLS-Fz2-C*; *+*; *24B-GAL4 / +*; *+*) or *imp-β11* mutant larvae (*w*, *UAS-myc-NLS-Fz2-C*; $imp\text{-}\beta11^{70}$ / *Df*; *24B-GAL4 / +*;+), nuclear staining was observed (**e**,**f**). Scale bar represents 10 μm.

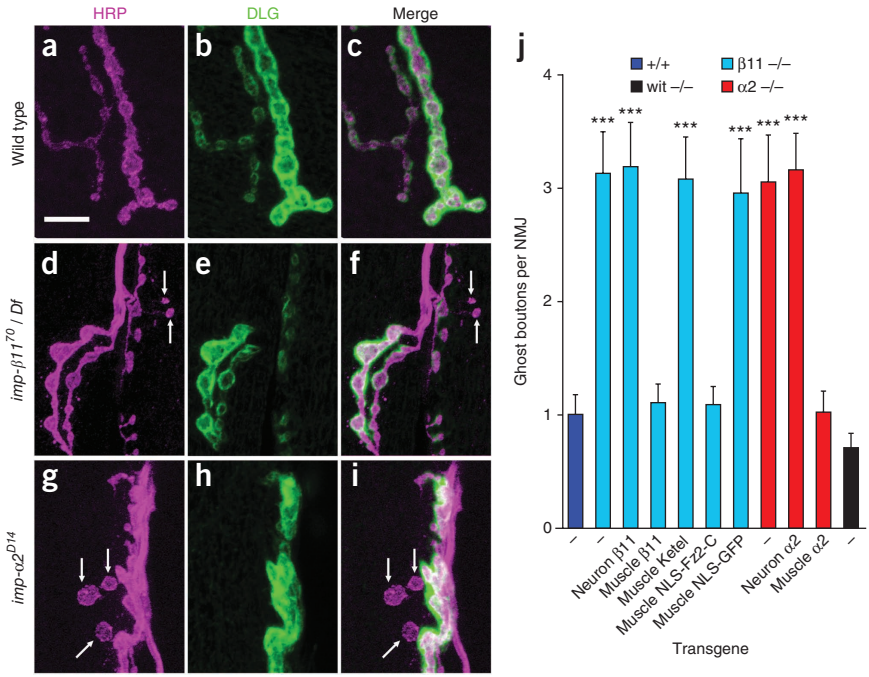

Figure 6 Ghost boutons are more frequent at *imp-β11* and *imp-α2* mutant NMJs. (**a**–**i**) Antibodies to HRP (magenta) and DLG (green) marked pre- and postsynaptic compartments of NMJs at muscles 6 and 7 of the indicated genotypes. Typically, each wild-type presynaptic bouton correctly faced a postsynaptic concentration of DLG, but, particularly in the mutant genotypes, there was an increased frequency of presynaptic boutons that had no opposite postsynaptic DLG (arrows). At other mutant boutons, DLG staining was weaker, but was still present. Wild type (*y,w*; *FRT42D*; +; +), *imp-β11* (*y,w*; *imp-β11*^{70} / *Df*; +; +), *imp-α2* mutant (*y,w*; *imp-α2*^{D14}; +; +). Scale bar represents 5 μm. (**j**) Loss of either Importin-β11 or Importin-α2 caused a threefold increase in ghost boutons. The frequency of ghost boutons could be returned to control levels by expression of the particular importin in the muscle, but not in neurons. Also, muscle expression of NLS-Fz2-C rescued the *imp-β11* phenotype, but a control NLS-tagged *GFP* transgene did not. Ghost boutons were quantified; genotypes (as indicated by colors) are as follows: +/+ (*y,w*; *FRT42D*; +; +); β11 –/– (*y,w*; *imp-β11*^{70} / *Df*; +; +); α2 –/– (*y,w*; *imp-α2*^{D14}; +; +); wit –/– (*y,w*; +; *wit*$^{A12/B11}$; +); β11 –/– Neuron β11 (*y,w*; *imp-β11*^{70} / *Df*; *elav-GAL4* / *UAS–imp-β11–eGFP*; +); β11 –/– Muscle β11 (*y,w*; *imp-β11*^{70} / *Df*; *24B-GAL4* / *UAS–imp-β11–eGFP*; +); α2 –/– Neuron α2 (*y,w*; *imp-α2*^{D14}; *elav-GAL4* / *UAS-imp-α2*; +); α2 –/– Muscle α2 (*y,w*; *imp-α2*^{D14}; *24B-GAL4* / *UAS-imp-α2*; +); β11 –/– Muscle Ketel (*y,w*; *imp-β11*^{70} / *Df*; *24B-GAL4* / *UAS-Ketel*; +); β11 –/– Muscle NLS-Fz2-C (*w*, *UAS-myc-NLS-Fz2-C* / + *or Y*; *imp-β11*^{70} / *Df*; *24B-GAL4* / +; +); β11 –/– Muscle NLS-GFP (*y,w*; *imp-β11*^{70} / *Df*; *UAS-NLS-GFP* / *24B-GAL4*; +). *** $P < 0.0001$ versus +/+. Error bars represent s.e.m.

We also examined muscles 6 and 7 expressing myc-NLS–Fz2-C via the BG487 GAL4 driver in a *dfz2* mutant background. This expression completely rescued the increase in ghost boutons associated with the loss of Fz2 function (**Supplementary Fig. 5**), indicating that the C terminus of Fz2 was sufficient to restore proper postsynaptic development. Thus Wingless, Fz2 and particularly Fz2-C are required for preventing errors in postsynaptic specializations.

Nuclear Fz2-C promotes correct postsynaptic specializations

We examined *imp-β11* and *imp-α2* mutants to determine whether ghost boutons arise from a failure of nuclear Fz2-C import (**Fig. 6**) and found their frequency increased more than threefold over controls (**Fig. 6j**). Although *imp-β11* mutants have fewer boutons[16], an increase in ghost boutons was not a secondary consequence of fewer boutons; null mutants in *wishful thinking*, the type II BMP receptor, had 50% fewer boutons[27,28], but no increase in the number of ghost boutons ($P > 0.2$; **Fig. 6j**).

To determine whether the lack of Importin-β11 and Importin-α2 in the nerve or muscle gave rise to this phenotype, we restored their expression in a tissue-specific manner. Muscle expression ($P < 0.0001$), but not neuronal expression ($P > 0.4$), corrected the ghost bouton phenotype (**Fig. 6j**). Ketel (Importin-β1) was unable to substitute for Importin-β11, as the number of ghost boutons was increased by more than threefold in *imp-β11* mutants overexpressing Ketel in muscle (P versus *imp-β11* > 0.7; **Fig. 6j**). Thus, Importin-β11 and Importin-α2 are required in the muscle to prevent ghost boutons.

If nuclear Fz2-C promotes proper postsynaptic development, then restoring it to *imp-β11* mutant muscles should restore normal development. Although transgenic Importin-β11 expression likely restored import of all Importin-β11–dependent cargoes, expression of myc-NLS-Fz2-C should restore only Fz2-C nuclear import (**Fig. 5**). Consistent with this hypothesis, muscle expression of myc-NLS–Fz2-C completely prevented the increase in ghost boutons in *imp-β11* mutants (P versus *imp-β11* < 0.0001, P versus +/+ > 0.7; **Fig. 6j**). This rescue was specific to Fz2-C; NLS-tagged GFP expression did not rescue the ghost bouton phenotype (P versus *imp-β11* > 0.4; **Fig. 6j**). These findings support a model in which Fz2-C nuclear import by Importin-β11 and Importin-α2 promotes proper postsynaptic development.

importin-β11 and *dfz2* mutants have a thinner SSR

Although the significant increase ($P < 0.0001$) in the number of ghost boutons that we observed indicates that Fz2-C import is important for postsynaptic development, ghost boutons represent a small percentage of the boutons at the NMJ (approximately 1% in wild type and 3% in the *imp-β11*, *imp-α2* or *dfz2* mutants). Their occurrence, therefore, was unlikely, in and of itself, to have a major effect on synaptic function. We hypothesized instead that the complete lack of DLG immunoreactivity at the ghost boutons reflected only the most

Table 1 Quantification of electron microscopy bouton parameters in third instar control and *imp-β11* mutant larvae

Genotype	Vesicle density (vesicles per μm^2)	PSD length (nm)	Percentage of mitochondrial area	Vesicle diameter (nm)	SSR crossings (crossings per nm)	Percentage of active zone length	T bars per active zone
Wild type	184.4 ± 22.55	610.0 ± 38.79	7.1 ± 0.80	33.17 ± 0.8109	0.013 ± 0.0013	31 ± 2.3	0.33 ± 0.094
imp-β11^{70} / *Df*	185.0 ± 23.99	577.8 ± 54.28	8.3 ± 2.0	34.52 ± 0.6966	0.015 ± 0.00079	35 ± 2.3	0.26 ± 0.067
	$P > 0.9$	$P > 0.6$	$P > 0.7$	$P > 0.2$	$P > 0.2$	$P > 0.2$	$P > 0.5$

Quantification of these parameters from type Ib boutons imaged by transmission electron microscopy. $n > 10$ boutons for both genotypes.

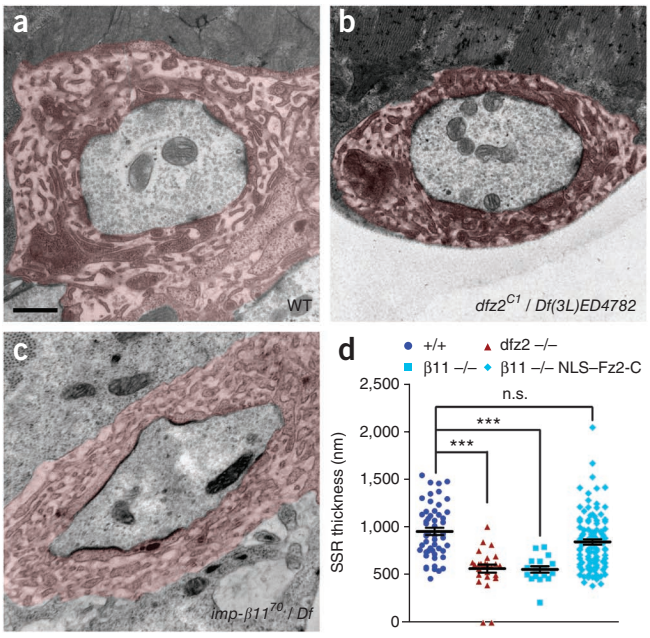

Figure 7 Loss of nuclear Fz2-C leads to reduced SSR thickness at the electron microscopy level. (**a**–**c**) Representative electron micrographs of type Ib boutons on muscles 6 and 7 in segment A2 of wild type (*y,w*; *FRT42D*; *+*; *+*), *imp-β11* mutants (*y,w*; *imp-β11*^{70} / *Df*; *+*; *+*) and *dfz2* mutants (*y,w*; *+*; *dfz2*^{C1} / *Df(3L)ED4782*; *+*). Both *imp-β11* and *dfz2* mutants display regions of SSR (false colored in red) that are thinner than wild-type controls. Scale bar represents 500 nm. (**d**) Scatterplot quantification of the thickness of the SSR in wild type (dark blue circles, *y,w*; *FRT42D*; *+*; *+*), *dfz2* mutants (crimson triangles, *y,w*; *+*; *dfz2*^{C1} / *Df(3L)ED4782*; *+*), *imp-β11* mutants (light blue squares, *y,w*; *imp-β11*^{70} / *Df*; *+*; *+*) and *imp-β11* mutants expressing NLS–Fz2-C in the muscle (light blue diamonds, *w*, *UAS-myc-NLS-Fz2-C*; *imp-β11*^{70} / *Df*; *24B-GAL4* / *+*). Each symbol represents the average thickness around a single bouton. Restoration of nuclear Fz2-C in the *imp-β11* mutant rescued SSR thickness to nearly wild-type levels. Specific values are as follows: *+/+* = 956.4 ± 38.66 nm, *n* = 5 animals, 52 boutons; β11 –/– (y,w; *imp-β11*^{70} / *Df*; +; +) = 558.5 ± 33.74 nm, *n* = 5 animals, 17 boutons; dfz2 –/– (y,w; +; *dfz2*^{C1} / *Df(3L)ED4782*; *+*) = 567.1 ± 41.71 nm, *n* = 3 animals, 26 boutons, *p* versus *imp-β11*^{70} / *Df* > 0.8; β11 –/– Muscle NLS-Fz2-C = 841.3 ± 28.72 nm, *n* = 5 animals, 103 boutons, *p* versus +/+ > 0.2, versus *imp-β11*^{70} / *Df* < 0.0001. *** *P* < 0.0001. Error bars represent s.e.m.

extreme example of a more widespread alteration. An indication of a more general consequence of Wingless signaling has been reported for *wg*^{TS} mutants raised with a temperature shift during larval development; at third instar, a third of their synaptic boutons lacked SSR, as determined by electron microscopy[14]. We therefore examined synaptic boutons by electron microscopy for defects resulting from impaired nuclear import of Fz2-C.

Presynaptic boutons in *imp-β11* mutants were ultrastructurally normal with regard to many parameters (**Table 1**). However, the SSR surrounding *imp-β11* and *dfz2* boutons (**Fig. 7a–c**) was only 58% as thick as that in controls (**Fig. 7d**). Similar reductions were seen in SSR area and the ratio of SSR area to bouton area, but not in the bouton area itself (**Supplementary Fig. 6**). The density, however, of SSR folds was unchanged (**Table 1**). Moreover, the phenotypes of *imp-β11* and *dfz2* were statistically indistinguishable. Of 26 *dfz2* boutons, two lacked any surrounding SSR (**Supplementary Fig. 7**), potentially an ultrastructural correlate of ghost boutons and similar to those observed in *wg*^{TS} larvae[14]. Although no boutons were seen that completely lacked SSR in *imp-β11* mutants, many had very little and might have been scored as ghost boutons by immunocytochemistry (**Supplementary Fig. 7**). This loss of SSR was not a result of a general defect in muscle growth or membrane traffic. Muscle size, input resistance and miniature excitatory postsynaptic potential amplitude in *imp-β11* larvae were all unchanged[16]. Moreover, despite thinner SSR, glutamate receptor levels were normal (**Supplementary Fig. 8**) and receptors correctly apposed active zones[16] everywhere except the ghost boutons. Thus, the SSR reduction is not an indication of broadly compromised muscles.

The reduced SSR in *imp-β11* and *dfz2* mutants suggests that import of Fz2-C promotes SSR growth. To address this hypothesis, we expressed myc-NLS–Fz2-C in *imp-β11* mutant muscles. As with the ghost bouton phenotype (**Fig. 6d**), this transgene nearly completely rescued the SSR defects (**Fig. 7d** and **Supplementary Fig. 7**). The ability of myc-NLS–Fz2-C to permit nuclear localization of Fz2-C and thereby overcome the *imp-β11* phenotype demonstrates that import of Fz2-C, and not other possible Importin-β11 cargoes, is required for full SSR development.

The role of nuclear Fz2-C and the identity of potential genes it might regulate are unknown. To address possible downstream factors in SSR growth, we immunocytochemically assayed a number of NMJ components that were previously shown to affect SSR thickness through either loss-of-function mutations or overexpression, including Wsp, dPix, dPak, Syndapin, PAR-1 and pDLG^{S797}, the target of PAR-1 (refs. 29–32). The fluorescence intensities of immunoreactivity for each of these were not detectably different between wild-type and *imp-β11* mutant NMJs (**Supplementary Fig. 9**), nor were protein levels in body-wall homogenates (data not shown). The SSR phenotype of *dfz2* and *imp-β11* mutants is likely to develop slowly during the third instar and may therefore arise from a relatively modest alteration in these or other factors governing SSR growth.

We also examined α-spectrin at the NMJ, as postsynaptic pools of α- and β-spectrin are required for SSR development and spectrin is enriched around each bouton[32,33]. The location of this spectrin relative to the membranes of the SSR is unknown, but spectrin may be an organizing scaffold for the SSR cytoskeleton. We observed a 23% reduction in the intensity of α-spectrin immunoreactivity at the NMJ in *imp-β11* larvae compared with controls (**Supplementary Fig. 10**). This decrease was accompanied by a 42% reduction in the thickness of α-spectrin staining surrounding the type Ib boutons (**Supplementary Fig. 10**). This thinning of α-spectrin is consistent with that of the SSR measured by electron microscopy and corroborates the finding of impaired postsynaptic development in the *imp-β11* mutant.

DISCUSSION

Both pre- and postsynaptic events shape the properties of synapses during their development and subsequent plastic changes. We examined a synapse-to-nucleus pathway that governs the anatomical maturation of the *Drosophila* neuromuscular junction, a model glutamatergic synapse. By analyzing the phenotypes of *imp-β11* and *imp-α2* mutants, we determined the mechanism by which an activity-dependent synaptic signal, the Fz2-C terminus, enters postsynaptic nuclei. By selectively blocking this process, we found that nuclear translocation caused growth of the SSR, a specialized postsynaptic membrane. By circumventing the importins with an NLS-tagged C-terminal peptide (NLS–Fz2-C), we found that this phenotype depended on this signal and not on other, unidentified nuclear cargoes that might use these importins.

Wingless signaling at the *Drosophila* NMJ is an activity-dependent process that involves secretion of the Wingless ligand from nerve terminals[12,14]. Activation of Fz2 receptors on the postsynaptic membrane may give rise to multiple signals in the muscle, but selective

block of one such signal, the nuclear import of Fz2-C, gave rise to a thinner SSR surrounding the terminals and more boutons that were not surrounded by the scaffold protein DLG. The SSR is an exceptional structure in which the sarcolemma is extensively invaginated[15]. The function of the SSR is unclear, but it may create biochemically isolated postsynaptic compartments, similar to dendritic spines[34]. By increasing the extracellular volume at the synapse, it may also provide a sink into which released glutamate can diffuse to terminate synaptic responses[15]. The SSR may filter the electrophysiological consequences of receptor activation[35] or otherwise alter electrical signals[36]. The SSR is also closely associated with ribosomes and may be a site of local glutamate receptor translation[37]. The SSR is absent from newly formed embryonic synapses and grows during the larval stages[38]. The number of boutons also increases during larval life and increased neuronal activity causes further increases in bouton number[39]. Thus, SSR growth entails the elaboration of postsynaptic membranes in an ongoing process at both existing synapses and newly added boutons. The activity-dependent secretion of Wingless and nuclear translocation of Fz2-C may therefore assist in matching SSR growth to synapse expansion. However, the SSR is reduced by only 42% in the absence of nuclear Fz2-C. Therefore, this signaling pathway serves to upregulate a process that is probably initiated by other signals. At present, the nuclear targets of Fz2-C are unknown and, in addition to the potentially subtle modulation of SSR component expression, may include unrelated targets that require modulation by presynaptically released Wingless.

Diminished SSR did not represent a broader impairment of muscle growth or membrane trafficking. Many muscle parameters, such as size, input resistance and quantal response[16], as well as glutamate receptor clustering (**Supplementary Fig. 8**) were normal. This latter observation is consistent with previous studies showing that receptors cluster at embryonic synapses before formation of the SSR[40] and independent of transmitter release[41]. Considerable receptor addition also occurs later as synapses are strengthened and new boutons form. This process was not blocked by *imp-β11* mutations or the loss of nuclear Fz2-C. Thus, the reduction in SSR is probably not a result of impaired muscle health, but is instead a result of a specific impairment of one aspect of synaptic maturation.

Nuclear import of Fz2-C requires an active process

Both Importin-β11 and Importin-α2 were required in the muscle for Fz2-C import and we detected both in a complex with Fz2, suggesting a direct role for both importins in nuclear Fz2-C import. Although Importin-α is chiefly found to interact with Importin-β1, we found that Importin-α2 partnered with Importin-β11 and Importin-β1 could not substitute for it. Thus, particular combinations of α and β importins may provide specificity to nuclear translocation of signals[42]. Notably, *cdm* (Importin-13) mutants also have diminished SSR[43]. We observed increased ghost boutons and decreased nuclear Fz2-C in *cdm* larvae (data not shown), suggesting that the active nuclear import complex may also contain this importin. As it has not yet been possible to determine whether there is a biochemical association of Importin-13 with the Fz2 receptor, its exact relationship remains uncertain.

Active nuclear import is not mandated by the size of Fz2-C (8 kDa), which is below the diffusionary limit for the nuclear pore[3]. Diffusion may account for the ~10% of normal levels of Fz2-C puncta that are observed in the absence of the importin, but is insufficient to preserve normal SSR growth. The inadequacy of free diffusion may indicate that cytosolic Fz2-C is restrained by a binding partner and an active import system may help to regulate the pathway. Such a step is implied by the finding that Fz2 is constitutively cleaved, but is thought to require an unidentified Wingless-triggered activation step for nuclear entry[10]. Recruitment of the importins in response to Wingless could represent this activation step. Indeed, when expressed in S2 cells, Fz2-C was cleaved and could interact with dGRIP, but did not enter the nucleus[10] or bind the importins in the absence of Wingless (**Supplementary Fig. 11**)[11].

Postsynaptic versus presynaptic Fz2-C phenotypes

Mutations of the Wnt pathway cause several NMJ phenotypes, including changes in bouton number, shape and presynaptic microtubule arrangements, in addition to the appearance of ghost boutons and the disruption of SSR formation reported here. Determining the mechanisms for each has therefore been complicated. For example, mutation of the Fz2 cleavage site[10] may disrupt other downstream pathways because the cleavage site is also a Disheveled (Dsh) binding site[44]. It has been suggested that a broad array of defects arose from the failure of Fz2-C nuclear import[10]. However, more recent work[13] found that bouton number, size and microtubule organization was predominantly, although not necessarily exclusively, controlled by a presynaptic and local Wnt signaling pathway similar to the mammalian cerebellum[45]. This leaves the importance of nuclear Fz2-C and other potential Fz2-derived muscle signals unresolved. Our identification of a nuclear import mechanism for Fz2-C allowed a separation of postsynaptic pathways and a directed assessment of nuclear Fz2-C in synaptic development (**Supplementary Fig. 12**).

Both *imp-β11* and *imp-α2* mutants caused errors in postsynaptic development that resemble defects associated in *wg* and *dfz2*: the increase in boutons lacking DLG (**Fig. 6** and **Supplementary Fig. 5**) and the underdevelopment of the SSR (**Fig. 7**). In contrast, neither *imp-β11* nor *imp-α2* mutants had the altered bouton size or cytoskeleton seen in *wg* and *dfz2* mutants (**Supplementary Fig. 4**). Only development of the SSR was consistently linked to failures in Fz2-C nuclear import. The restoration of normal postsynaptic development by myc-NLS–Fz2-C in *dfz2* and *imp-β11* mutants confirmed that nuclear Fz2-C is necessary and sufficient for normal postsynaptic development in these mutant backgrounds (**Supplementary Fig. 12**).

Fz2-C import may not fully account for Wingless signaling in the muscle; nearly one-third of boutons in *wg* mutants completely lacked SSR[14], whereas nearly all of the boutons in *dfz2* and *imp-β11* mutants retained some SSR. A likely explanation is the presence of a parallel pathway mediated by another Wingless receptor, Frizzled, and Dsh. Dsh is present in muscle[13] and we observed Frizzled immunoreactivity at the NMJ (data not shown). Indeed, partial redundancy of Frizzled and Fz2 exists in embryonic patterning[18]. Because Armadillo/β-catenin, the nucleus-targeted element of the canonical Wnt pathway, is not detectable in the muscle[13], the Frizzled/Dsh pathway may be local and cytoplasmic. It is tempting to speculate that the two pathways work in parallel, with the Frizzled/Dsh-dependent pathway driving SSR formation locally and Fz2-C supporting it in the nucleus via transcriptional changes.

The nuclear translocation of a synaptic Fz2-C signal illustrates the importance of synapse-to-nucleus signaling and active nuclear import for synaptic development. This mode of signaling also occurs for learning and memory models and axonal regeneration[2,4]. Receptor cleavage and nuclear translocation are well-established for many developmental signals, but have chiefly been identified in single-pass transmembrane proteins[9,46]. For the seven transmembrane domain Frizzled receptors, however, the *Drosophila* NMJ is the only known model. Wnt signaling influences synapse formation in mammalian brain and Fz5 and Fz8, the closest mammalian homologs of *Drosophila* Fz2, are strongly expressed in the hippocampus[47]. Both Fz5 and Fz8 are highly conserved with *Drosophila* Fz2 in the vicinity

of the cleavage site and also have extended C-terminal sequences[48]. Potentially, the signaling pathway that promotes postsynaptic development in *Drosophila* via Wnt signaling, receptor cleavage and active nuclear import of the C terminus may also occur in mammals. As at the fly NMJ, mammalian nuclear import factors are likely regulators of synapse-to-nucleus signals rather than passive facilitators of transit through the nuclear pore. By associating with synaptic receptors in a manner likely to depend on receptor activation, importins offer a means for coordinating gene regulation with synaptic activity.

METHODS

Methods and any associated references are available in the online version of the paper at http://www.nature.com/natureneuroscience/.

Note: Supplementary information is available on the Nature Neuroscience website.

ACKNOWLEDGMENTS

We gratefully acknowledge V. Budnik and colleagues for generously providing antibodies and fly stocks and helpful discussions. We thank S. Cotterrill, R. Fleming, I. Kiss, P. Macdonald, B. Mechler, H. Bellen, M. Noll, M. Ramaswami, H. Saumweber, D. Schmucker, G. Struhl, J. Szabad, J.P. Vincent, S. Wasserman, Y. Jan, L. Zipursky, the Bloomington Stock Center and the Developmental Studies Hybridoma Bank for fly stocks and antibodies. We also thank M. Kovtun and members of the Schwarz laboratory for helpful discussions and critical readings of the manuscript, as well as M. Liana and L. Bu of the Intellectual and Developmental Disability Research Center Histology (grant number P30HD18655) and Imaging Cores for technical assistance. This work was supported by US National Institutes of Health grants RO1 NS041062 and MH075058 (T.L.S.) and a predoctoral fellowship from the National Defense Science and Engineering Graduate Foundation (T.J.M.).

AUTHOR CONTRIBUTIONS

T.J.M. performed the experiments and analyzed the data. T.J.M. and T.L.S. designed the experiments and wrote the paper.

COMPETING FINANCIAL INTERESTS

The authors declare no competing financial interests.

Published online at http://www.nature.com/natureneuroscience/.
Reprints and permissions information is available online at http://www.nature.com/reprintsandpermissions/.

1. Jordan, B.A. & Kreutz, M.R. Nucleocytoplasmic protein shuttling: the direct route in synapse-to-nucleus signaling. *Trends Neurosci.* **32**, 392–401 (2009).
2. Otis, K.O., Thompson, K.R. & Martin, K.C. Importin-mediated nuclear transport in neurons. *Curr. Opin. Neurobiol.* **16**, 329–335 (2006).
3. Weis, K. Nucleocytoplasmic transport: cargo trafficking across the border. *Curr. Opin. Cell Biol.* **14**, 328–335 (2002).
4. Perry, R.B. & Fainzilber, M. Nuclear transport factors in neuronal function. *Semin. Cell Dev. Biol.* **20**, 600–606 (2009).
5. Thompson, K.R. *et al.* Synapse to nucleus signaling during long-term synaptic plasticity; a role for the classical active nuclear import pathway. *Neuron* **44**, 997–1009 (2004).
6. Ting, C.Y. *et al.* Tiling of r7 axons in the *Drosophila* visual system is mediated both by transduction of an activin signal to the nucleus and by mutual repulsion. *Neuron* **56**, 793–806 (2007).
7. Salinas, P.C. & Zou, Y. Wnt signaling in neural circuit assembly. *Annu. Rev. Neurosci.* **31**, 339–358 (2008).
8. Cadigan, K.M. Wnt-beta-catenin signaling. *Curr. Biol.* **18**, R943–R947 (2008).
9. Lyu, J., Yamamoto, V. & Lu, W. Cleavage of the Wnt receptor Ryk regulates neuronal differentiation during cortical neurogenesis. *Dev. Cell* **15**, 773–780 (2008).
10. Mathew, D. *et al.* Wingless signaling at synapses is through cleavage and nuclear import of receptor DFrizzled2. *Science* **310**, 1344–1347 (2005).
11. Ataman, B. *et al.* Nuclear trafficking of *Drosophila* Frizzled-2 during synapse development requires the PDZ protein dGRIP. *Proc. Natl. Acad. Sci. USA* **103**, 7841–7846 (2006).
12. Ataman, B. *et al.* Rapid activity–dependent modifications in synaptic structure and function require bidirectional Wnt signaling. *Neuron* **57**, 705–718 (2008).
13. Miech, C., Pauer, H.U., He, X. & Schwarz, T.L. Presynaptic local signaling by a canonical wingless pathway regulates development of the *Drosophila* neuromuscular junction. *J. Neurosci.* **28**, 10875–10884 (2008).
14. Packard, M. *et al.* The *Drosophila* Wnt, wingless, provides an essential signal for pre- and postsynaptic differentiation. *Cell* **111**, 319–330 (2002).
15. Rheuben, M.B., Yoshihara, M. & Kidokoro, Y. Ultrastructural correlates of neuromuscular junction development. *Int. Rev. Neurobiol.* **43**, 69–92 (1999).
16. Higashi-Kovtun, M.E., Mosca, T.J., Dickman, D.K., Meinertzhagen, I.A. & Schwarz, T.L. Importin-beta11 regulates synaptic phosphorylated mothers against decapentaplegic and thereby influences synaptic development and function at the *Drosophila* neuromuscular junction. *J. Neurosci.* **30**, 5253–5268 (2010).
17. Goldfarb, D.S., Corbett, A.H., Mason, D.A., Harreman, M.T. & Adam, S.A. Importin alpha: a multipurpose nuclear-transport receptor. *Trends Cell Biol.* **14**, 505–514 (2004).
18. Chen, C.M. & Struhl, G. Wingless transduction by the Frizzled and Frizzled2 proteins of *Drosophila*. *Development* **126**, 5441–5452 (1999).
19. Menon, K.P., Andrews, S., Murthy, M., Gavis, E.R. & Zinn, K. The translational repressors Nanos and Pumilio have divergent effects on presynaptic terminal growth and postsynaptic glutamate receptor subunit composition. *J. Neurosci.* **29**, 5558–5572 (2009).
20. Cantera, R., Kozlova, T., Barillas-Mury, C. & Kafatos, F.C. Muscle structure and innervation are affected by loss of Dorsal in the fruit fly, *Drosophila melanogaster*. *Mol. Cell. Neurosci.* **13**, 131–141 (1999).
21. Piddini, E., Marshall, F., Dubois, L., Hirst, E. & Vincent, J.P. Arrow (LRP6) and Frizzled2 cooperate to degrade Wingless in *Drosophila* imaginal discs. *Development* **132**, 5479–5489 (2005).
22. Lange, A. *et al.* Classical nuclear localization signals: definition, function and interaction with importin alpha. *J. Biol. Chem.* **282**, 5101–5105 (2007).
23. Roos, J., Hummel, T., Ng, N., Klambt, C. & Davis, G.W. *Drosophila* Futsch regulates synaptic microtubule organization and is necessary for synaptic growth. *Neuron* **26**, 371–382 (2000).
24. Hummel, T., Krukkert, K., Roos, J., Davis, G. & Klambt, C. *Drosophila* Futsch/22C10 is a MAP1B-like protein required for dendritic and axonal development. *Neuron* **26**, 357–370 (2000).
25. Lahey, T., Gorczyca, M., Jia, X.X. & Budnik, V. The *Drosophila* tumor suppressor gene dlg is required for normal synaptic bouton structure. *Neuron* **13**, 823–835 (1994).
26. Marrus, S.B. & DiAntonio, A. Preferential localization of glutamate receptors opposite sites of high presynaptic release. *Curr. Biol.* **14**, 924–931 (2004).
27. Aberle, H. *et al.* wishful thinking encodes a BMP type II receptor that regulates synaptic growth in *Drosophila*. *Neuron* **33**, 545–558 (2002).
28. Marqués, G. *et al.* The *Drosophila* BMP type II receptor wishful thinking regulates neuromuscular synapse morphology and function. *Neuron* **33**, 529–543 (2002).
29. Parnas, D., Haghighi, A.P., Fetter, R.D., Kim, S.W. & Goodman, C.S. Regulation of postsynaptic structure and protein localization by the Rho-type guanine nucleotide exchange factor dPix. *Neuron* **32**, 415–424 (2001).
30. Zhang, Y. *et al.* PAR-1 kinase phosphorylates Dlg and regulates its postsynaptic targeting at the *Drosophila* neuromuscular junction. *Neuron* **53**, 201–215 (2007).
31. Coyle, I.P. *et al.* Nervous wreck, an SH3 adaptor protein that interacts with Wsp, regulates synaptic growth in *Drosophila*. *Neuron* **41**, 521–534 (2004).
32. Kumar, V. *et al.* Syndapin promotes formation of a postsynaptic membrane system in. *Drosophila*. *Mol. Biol. Cell* **20**, 2254–2264 (2009).
33. Pielage, J., Fetter, R.D. & Davis, G.W. A postsynaptic spectrin scaffold defines active zone size, spacing and efficacy at the *Drosophila* neuromuscular junction. *J. Cell Biol.* **175**, 491–503 (2006).
34. Nimchinsky, E.A., Sabatini, B.L. & Svoboda, K. Structure and function of dendritic spines. *Annu. Rev. Physiol.* **64**, 313–353 (2002).
35. Faeder, I.R. & Salpeter, M.M. Glutamate uptake by a stimulated insect nerve muscle preparation. *J. Cell Biol.* **46**, 300–307 (1970).
36. Wong, K., Karunanithi, S. & Atwood, H.L. Quantal unit populations at the *Drosophila* larval neuromuscular junction. *J. Neurophysiol.* **82**, 1497–1511 (1999).
37. Sigrist, S.J. *et al.* Postsynaptic translation affects the efficacy and morphology of neuromuscular junctions. *Nature* **405**, 1062–1065 (2000).
38. Guan, B., Hartmann, B., Kho, Y.H., Gorczyca, M. & Budnik, V. The *Drosophila* tumor suppressor gene, *dlg*, is involved in structural plasticity at a glutamatergic synapse. *Curr. Biol.* **6**, 695–706 (1996).
39. Mosca, T.J., Carrillo, R.A., White, B.H. & Keshishian, H. Dissection of synaptic excitability phenotypes by using a dominant-negative Shaker K^+ channel subunit. *Proc. Natl. Acad. Sci. USA* **102**, 3477–3482 (2005).
40. Chen, K. & Featherstone, D.E. Discs-large (DLG) is clustered by presynaptic innervation and regulates postsynaptic glutamate receptor subunit composition in *Drosophila*. *BMC Biol.* **3**, 1 (2005).
41. Pack-Chung, E., Kurshan, P.T., Dickman, D.K. & Schwarz, T.L. A *Drosophila* kinesin required for synaptic bouton formation and synaptic vesicle transport. *Nat. Neurosci.* **10**, 980–989 (2007).
42. Freedman, N.D. & Yamamoto, K.R. Importin 7 and importin alpha/importin beta are nuclear import receptors for the glucocorticoid receptor. *Mol. Biol. Cell* **15**, 2276–2286 (2004).
43. Giagtzoglou, N., Lin, Y.Q., Haueter, C. & Bellen, H.J. Importin 13 regulates neurotransmitter release at the *Drosophila* neuromuscular junction. *J. Neurosci.* **29**, 5628–5639 (2009).
44. Wong, H.C. *et al.* Direct binding of the PDZ domain of Dishevelled to a conserved internal sequence in the C-terminal region of Frizzled. *Mol. Cell* **12**, 1251–1260 (2003).
45. Ahmad-Annuar, A. *et al.* Signaling across the synapse: a role for Wnt and Dishevelled in presynaptic assembly and neurotransmitter release. *J. Cell Biol.* **174**, 127–139 (2006).
46. Ehebauer, M., Hayward, P. & Martinez-Arias, A. Notch signaling pathway. *Sci. STKE* **2006**, cm7 (2006).
47. Davis, E.K., Zou, Y. & Ghosh, A. Wnts acting through canonical and noncanonical signaling pathways exert opposite effects on hippocampal synapse formation. *Neural Dev.* **3**, 32 (2008).
48. Speese, S.D. & Budnik, V. Wnts: up-and-coming at the synapse. *Trends Neurosci.* **30**, 268–275 (2007).

ONLINE METHODS

Drosophila stocks. All *Drosophila* strains were raised at 25 °C. All mutants and transgenes were examined in a *y*, *w* background and maintained over GFP balancer chromosomes. The isogenic parental stock *y*, *w*; *FRT42D* was used as the wild-type control. The following alleles were used: eag^1Sh^{KS133}, wit^{A12}, wit^{B11}, $dfz2^{C1}$, Df(3L)ED4782 uncovering *dfz2*, wg^{IL114} (referred to here as wg^{TS}), wg^1, $imp\text{-}\alpha2^{D3}$, $imp\text{-}\alpha2^{D14}$, Df(3L)α1S1 uncovering *Kap-α1*, dl^1, $imp\text{-}\beta11^{70}$, and Df(2R)Δm22 uncovering *importin-β11*. Allele sources and references are detailed in **Supplementary Table 1**. wg^{TS} larvae were raised at 18 °C until early third instar and then shifted to 30 °C for 18 h before dissection. The following transgenic strains were used: 24B-GAL4, Elav-GAL4, BG487-GAL4, UAS–Importin-β11–eGFP, UAS-DFz2-FLAG, UAS-Wingless, UAS-myc-NLS–DFz2-C, UAS-NLS-GFP and UAS–Importin-α2.

Immunohistochemistry. Wandering third instar larvae raised at low density were dissected and fixed for 20 min in fresh 4% paraformaldehyde (vol/vol, Sigma-Aldrich) in phosphate-buffered saline or for 5 min in Bouin's fixative (Sigma-Aldrich). Larvae were incubated overnight at 4 °C in primary antibodies and for 2 h at room temperature in secondary antibodies. The following primary antibodies were used: rabbit antibody to DFz2-C (1:200), rabbit antibody to DFz2-N (1:100), rat antibody to dGRIP (1:200), mouse antibody to DLG (1:500), rabbit antibody to Dorsal (1:1,000), rabbit antibody to FLAG (1:500, Sigma-Aldrich), mouse antibody to Futsch (1:50), rabbit antibody to Importin-α1 (1:100), rabbit antibody to Importin-α2 (1:100), rabbit antibody to Importin-α3 (1:100), rabbit antibody to Importin-β11 (1:750), rabbit antibody to Ketel (1:200), mouse antibody to Lamin C (1:200), rat antibody to Nanos (1:300), mouse antibody to nonA (1:100), rabbit antibody to Wingless (1:200), mouse antibody to Myc (1:300, Santa Cruz Biotechnology), mouse antibody to GluRIIA (1:100), rabbit antibody to GluRIIB (1:2,500), rabbit antibody to GluRIIC (1:2,000), mouse antibody to dPix (1:25), rabbit antibody to dPak (1:500), rabbit antibody to PAR-1 (1:100), rabbit antibody to $pDLG^{S797}$ (1:200), guinea pig antibody to Syndapin (1:500), guinea pig antibody to WASp (1:1,000) and mouse antibody to α-spectrin (1:50). Antibody sources and references are detailed in **Supplementary Table 2**. FITC-, Cy3- or Cy5-conjugated secondary antibodies were used at 1:200 (Jackson ImmunoResearch). Alexa488-, Alexa546- or Alexa647-conjugated secondary antibodies were used at 1:250 (Invitrogen). Cy3-, Cy5- or FITC-conjugated antibodies to horseradish peroxidase were used at 1:100 (Jackson ImmunoResearch). Larvae were mounted in Vectashield (Vector Laboratories) and stored at −20 °C until imaging.

Electron microscopy. Wandering third instar larvae were dissected as described above and internal organs were gently removed. Following dissection, the body walls, still pinned, were fixed at 4 °C overnight in 2.5% paraformaldehyde, 5.0% glutaraldehyde (vol/vol) and 0.06% picric acid (vol/vol) in 0.1 M cacodylate buffer, rinsed three times for 20 min in 0.1 M cacodylate buffer on ice, unpinned and post-fixed with 2% osmium tetroxide (vol/vol) in 0.1 M cacodylate buffer for 2 h on ice. They were then rinsed three times for 10 min in deionized water and dehydrated in an ethanol series (50%, 70%, 95%, 100% and 100%, vol/vol) and propylene oxide and placed overnight in 50% TAAB 712 Resin (vol/vol) in propylene oxide. They were transferred to fresh resin for 4 h and then embedded in fresh resin at 65 °C for 2 d or until hard. The 6/7 muscle region was located by eye and the block was trimmed around the desired area. Sections were taken parallel to the surface of the muscles: four 90-nm sections were collected as a series and then 3 μm of thick sections were removed before the next series of 90-nm sections. Sections were mounted on formvar-coated single slot grids, stained with lead and uranyl acetate, and imaged on a Tecnai G^2 Spirit BioTWIN (FEI Company) electron microscope at 11,000× and 30,000× magnification.

Imaging and statistical analysis. Larvae were imaged with a Zeiss LSM 510 Meta laser-scanning confocal microscope (Carl Zeiss) and either a 63× 1.4 NA or 40× 1.0 NA objective. Images of NMJs were taken as confocal *z* stacks with the upper and lower parameters determined by HRP immunoreactivity. Images of nuclei were taken as confocal *z* stacks with the parameters defined by either nonA or Lamin C staining. Images were processed with the LSM software, Adobe Photoshop CS2 or Microsoft PowerPoint. Ghost boutons were analyzed in confocal *z* stacks of an entire NMJ from muscles 6 and 7 in segments A2, A3 and A4 on the right and left sides and only counted if connected to the rest of the nerve. For comparisons of immunofluorescence, larvae were processed in the same tube and genotypes were imaged under identical conditions in the same session. Measurements of bouton diameters and the width of the spectrin-containing zone were determined from α-spectrin and HRP immunoreactivity. For each NMJ, four type Ib boutons were measured (two terminal and two internal) from the NMJ on muscle 4. From these boutons, width measurements were conducted on high-magnification images using ImageJ (US National Institutes of Health). The width of the spectrin zone was defined as the distance from the margin of the HRP-positive bouton to the outer margin of spectrin immunoreactivity and was experimentally determined by taking the diameter of spectrin immunoreactivity that surrounded the bouton, subtracting the diameter of the bouton and dividing by 2.

In electron micrographs, SSR thickness was calculated (ImageJ) only on boutons that contained vesicles, an active zone and subcellular organelles and were >1 μm in both length and width. An arbitrary center was chosen for each bouton and eight radii drawn at 45° angles; the SSR was measured along each line and averaged for each bouton. Bouton area and SSR area were measured by tracing the borders of both the bouton and the entire bouton and SSR in ImageJ. The SSR area was determined by subtracting the bouton area measurement from the full area measurement. Other parameters were determined as previously described[49]. Statistical analysis used GraphPad Prism 5 (Graphpad Software). In cases involving more than two samples, statistical significance was calculated using ANOVA followed by with a Dunnett *post hoc* test to the control sample. Where only two samples were compared, an unpaired Student's *t* test was used.

Fz2-C puncta were quantified as previously described[10–12]. Briefly, puncta were scored live on a Nikon E800 epifluorescence microscope as distinct spots of Fz2-C immunoreactivity over background staining at muscles 6 and 7 in segments A2 and A3 on both the right and left sides. In all cases, nuclei were positively identified by co-staining with antibodies to nonA and Lamin C or with DAPI.

Fluorescent intensity for glutamate receptors and postsynaptic molecules was measured in ImageJ. Confocal *z* stacks of the entire NMJ at muscle 4 were imported and converted into multi-channel composite images. A region of interest was drawn on the basis of the antibody to HRP channel and the mean fluorescence intensity measured in the other channels. In all genotypes, the average antibody to HRP fluorescence did not differ substantially, enabling direct comparison of the experimental labeling. For all comparisons, larvae were processed simultaneously and imaged under identical settings.

Immunoprecipitation. For each genotype, larval body walls from 20 wandering third instar larvae were dissected as described above, on ice, and drop-frozen in liquid nitrogen before homogenization on ice in 400 μl of lysis buffer (150 mM NaCl, 50 mM Tris-HCl (pH 7.5), 1% NP-40 (vol/vol), 1 mM EDTA, 100 μM Na_3VO_4, 10 mM NaF and a complete protease inhibitor tablet; Roche Applied Science). Debris was pelleted at 18,000*g* for 10 min at 4 °C. M2 antibody to FLAG–conjugated agarose beads (Sigma-Aldrich) were added to supernatants for 2 h at 4 °C and then washed extensively in lysis buffer. Proteins were then eluted at 95 °C.

Western Blots and SDS-PAGE Analysis. Proteins were separated on 8% polyacrylamide gels and transferred to nitrocellulose membrane. Primary antibodies were applied overnight at 4 °C and secondary antibodies for 1 h at 21–23 °C and diluted in blocking solution. The following primary antibodies were used: rabbit antibody to GFP (1:3,000, Invitrogen), rabbit antibody to GFP (1:5,000, AbCam), rabbit antibody to FLAG (1:5,000, Sigma-Aldrich), mouse antibody to FLAG (1:5,000, Sigma-Aldrich), rabbit antibody to Importin-α2 (1:2,000), mouse antibody to α-tubulin (1:25,000, Sigma-Aldrich), mouse antibody to Myc (1:1,000, Santa Cruz Biotechnology) and mouse antibody to V5 (1:2,500, Invitrogen). HRP-conjugated secondary antibodies were used at 1:10,000 (antibody to mouse primaries) or 1:20,000 (antibody to rabbit primaries) and were obtained from Jackson ImmunoResearch. Blots were developed using the SuperSignal West Dura Extended Duration Substrate Kit (Thermo Scientific).

S2 Cell Culture. *Drosophila* S2 cells were maintained at room temperature in Schneider's *Drosophila* medium (Invitrogen) containing 10% fetal bovine serum (vol/vol), penicillin (1 U ml^{-1}), streptomycin (1 μg ml^{-1}) and amphotericin B (2.5 ng ml^{-1}). The following constructs were used: pUAST-Importin-β11-eGFP[16], pAcpA-Actin5c-GAL4 (ref. 50), pAc5.1-Fz2-8xMyc-C[10], pAc5.1-dGRIP-V5 (ref. 11). Cells were transfected at 80% confluence using 1 μg of each plasmid (0.2 μg for pAcPa-Actin5c-GAL4) with the Effectene transfection reagent according to manufacturer's protocols (QIAgen). Cells were lysed in lysis buffer following 48-h

doi:10.1038/nn.2593

incubation and processed for immunoprecipitation as described above, with the following modification: supernatants were incubated for 2 h with antibody to Myc (Santa Cruz Biotechnology) and then with Protein A–conjugated Affi-Prep beads (Bio-Rad) for 1 h at 4 °C.

49. Wairkar, Y.P. *et al.* Unc-51 controls active zone density and protein composition by downregulating ERK signaling. *J. Neurosci.* **29**, 517–528 (2009).
50. McCabe, B.D. *et al.* The BMP homolog Gbb provides a retrograde signal that regulates synaptic growth at the *Drosophila* neuromuscular junction. *Neuron* **39**, 241–254 (2003).